Supplementary Material for

Scalable and Highly-Tunable Conductive Oxide Interfaces

Dana Cohen-Azarzar[1], Maria Baskin[1], Andreas Lindblad[2], Felix Trier[3], Lior Kornblum[1, a)]

[1]*The Andrew & Erna Viterbi Dept. of Electrical and Computer Engineering, Technion – Israel Institute of Technology, Haifa 32000-03 – Israel*
[2]*Department of Physics and Astronomy, Uppsala University, 752 36 Uppsala – Sweden*
[3]*Department of Energy Conversion and Storage, Technical University of Denmark, 2800 Kgs. Lyngby, Denmark*

Microstructural Analysis of Al_2O_3

X-ray diffraction (XRD) was acquired to verify the Al_2O_3 layer is not crystalline, using a Rigaku Smartlab diffractometer with a rotating anode source and a 2-bounce Ge (220) monochromator operated in 2θ/ω geometry (at a scan rate of 1 °/min). The diffraction was acquired for a 10 nm thick Al_2O_3 on STO. Figure S1 shows no discernable features other than the STO(001) and STO(002) Bragg peaks, confirming that the Al_2O_3 layer is amorphous within the detection limit.

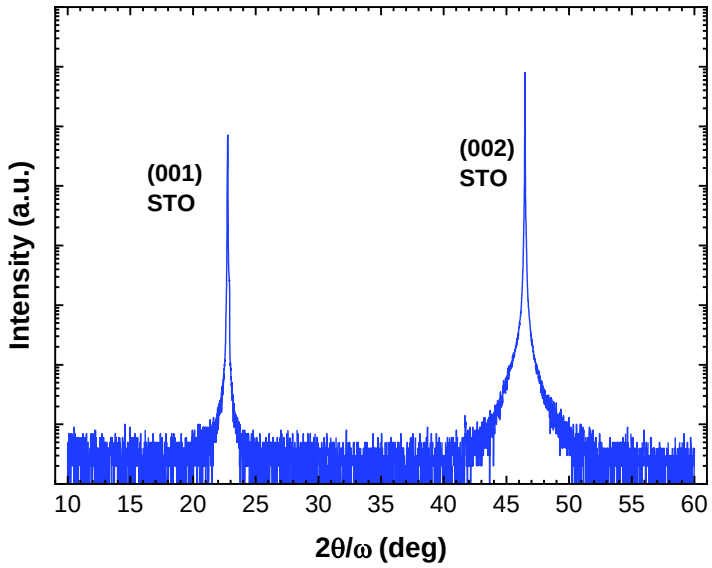

Figure S1. X-ray diffraction of 10 nm Al_2O_3 layer grown on an STO substrate.

Transport measurements – Room temperature screening

The 4 nm Al_2O_3 was grown on bare, TiO_2-terminated STO using ALD. NH_3 plasma was introduced for a different duration before the film deposition. Samples with the same exposure duration were grown in two separate batches. The first batch was for the resistance measurements; the second was grown at a later time for x-ray photoelectron spectroscopy (XPS) measurements. After the contact deposition, all the samples from the first batch (Table S1) were measured at room temperature in 2- and 4-point configurations for all possible configurations. These room temperature measurements were done in a light-sealed probe station. The resistances were extracted from the current-voltage (IV) curve slope, and they are summarized in Fig S1, and Table S1.

Some samples showed unexpected anisotropy of the 4-point resistance values. We define a sample to be "anisotropic" when it has an order of magnitude difference, or more, between the different 4-point configurations. We ascribe this behavior to the possibility of terrace edge conductivity[1], but we were unable to correlate this observation with the miscut direction. We note that this feature is more prevalent in the more resistive samples (Fig. S1), which could indicate a percolation of conductive regions near the metal-insulator transition (Fig. 2a). Samples that are deemed anisotropic were not considered further in this study.

From the isotropic samples, we then select a representative sample from each batch (blue squares in Fig. S1). For the 1 min set – the measured resistance for 3 out of 4 samples is abnormally high (versus our expectations based on previous growths). Sample DC198 behaved as expected. To validate its selection, we ran an additional identical 1 min growth on four substrates (DC216-219, orange stars in Fig S1), which were consistent with both our expectations and DC198. After this validation, we used DC198 from the original series. These representative samples were bonded with Au wires and underwent variable temperature transport measurements using a physical properties measurement system (PPMS), Figures 2, S2 and S3.

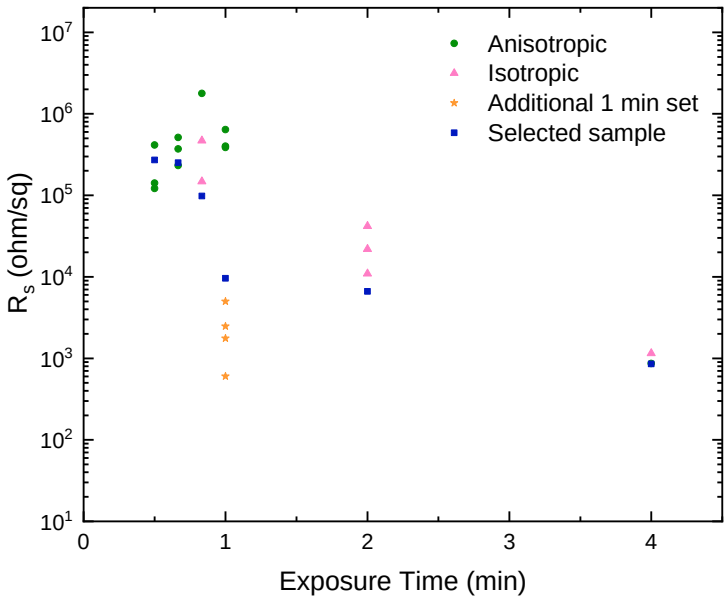

Figure S2. Room temperature sheet resistance as a function of the NH_3 plasma durations for all the samples from the electrical measurement batch.

Table S1. 2-point (2P), 4-point (4P), and contact resistance (R_C) for the experiment for all samples (Fig. S1). "2P 12" refers to a 2-point configuration where the current flows between contacts 1 and 2. "4P 1" refers to the 1st configuration out of 4 possible configurations in 4-point configurations. R is the average resistance of the 4P measurements. 4P Rs is $R \cdot \pi / \ln(2)$ where R is the average of the 4P configurations. "Rc 12" refers to the average resistance of contacts 1 and 2. Pink denotes data that was not used due to an anisotropy of an order of magnitude or more between the 4P configurations.

Exposure Duration (sec)	Wafer name	2p 12 Ω	2p 14 Ω	2p 23 Ω	2p 34 Ω	4p 1 Ω	4p 2 Ω	4p 3 Ω	4p 4 Ω	R Ω	4P Rs Ω/sq.	Rc 12 Ω	Rc 14 Ω	Rc 23 Ω	Rc 34 Ω
30	DC188	189,171	234,711	196,722	253,572	33,967	33,976	28,270	28,273	31,122	141,054	79,025	101,795	82,800	111,225
	DC189	365,881	394,413	454,365	504,909	66,638	66,685	53,115	53,172	59,902	271,499	152,989	167,255	197,231	222,503
	DC190	919,743	549,702	1,396,999	1,011,111	86,790	86,922	96,309	96,317	91,585	415,095	414,079	229,058	652,707	459,763
	DC191	144,173	178,151	144,634	175,471	25,758	25,762	27,908	27,915	26,836	121,630	58,669	75,658	58,899	74,318
40	DC204	519,493	431,390	581,678	557,982	98,098	98,020	65,434	65,437	81,747	370,507	218,873	174,822	249,965	238,118
	DC205	362,830	287,110	397,617	345,774	58,442	58,442	44,227	44,229	51,335	232,668	155,747	117,888	173,141	147,219
	DC206	316,784	203,416	352,310	294,596	72,410	72,481	38,429	38,433	55,438	251,265	130,673	73,989	148,436	119,579
	DC207	769,858	641,417	908,000	756,011	113,384	113,371	113,389	113,434	113,394	513,944	328,232	264,012	397,303	321,308
50	DC208	47,879	103,966	253,796	62,789	338	335	206,079	206,149	103,225	467,854	(27,673)	371	75,286	(20,218)
	DC209	101,236	32,332	24,673	48,695	65,134	65,149	52	52	32,596	147,739	34,320	(132)	(3,962)	8,049
	DC210	665,239	613,388	55,222	61,940	36,556	36,556	6,713	6,690	21,629	98,029	321,805	295,879	16,797	20,156
	DC211	918,311	3,178,083	2,091,603	4,228,941	387,741	386,359	398,954	399,022	393,019	1,781,304	262,646	1,392,532	849,292	1,917,961
60	DC192	19,713	10,126	21,402	15,179	3,055	3,054	1,184	1,183	2,119	9,604	8,797	4,004	9,641	6,530
	DC193	650,369	565,291	621,389	533,256	84,392	84,496	86,380	86,374	85,411	387,111	282,479	239,940	267,989	223,923
	DC194	369,116	1,860,964	524,367	572,666	80,955	80,964	96,179	96,219	88,579	401,473	140,268	886,192	217,894	242,043
	DC195	841,178	907,206	757,568	889,615	151,873	151,854	131,095	131,187	141,502	641,338	349,838	382,852	308,033	374,057
120	DC196	41,683	24,750	17,676	26,092	16,901	16,901	1,574	1,574	9,238	41,868	16,223	7,756	4,219	8,427
	DC197	17,991	12,518	10,852	20,998	9,408	9,408	253	253	4,831	21,894	6,580	3,844	3,011	8,084
	DC198	8,404	9,248	10,391	6,990	320	320	2,600	2,601	1,460	6,618	3,472	3,894	4,465	2,765
	DC199	8,638	7,930	9,552	3,938	27	27	4,808	4,802	2,416	10,950	3,111	2,757	3,568	761
240	DC200	1,614	2,155	2,767	1,980	32	32	477	477	255	1,154	679	950	1,256	863
	DC201	2,095	1,853	1,868	1,218	71	71	307	306	189	854	953	832	840	515
	DC202	1,504	1,467	2,557	2,018	56	56	325	325	190	863	657	638	1,183	914
Additional 60	DC216	1,406	1,117	918	821	181	181	85	85	133	603	636	492	392	344
	DC217	2,277	2,496	4,025	2,571	63	63	1,029	1,029	546	2,473	866	975	1,740	1,013
	DC218	3,606	1,365	1,856	2,910	2,133	2,134	71	71	1,102	4,996	1,252	131	377	904
	DC219	1,055	4,282	2,485	2,697	53	53	723	723	388	1,758	333	1,947	1,048	1,154

Possible effect of ambient light

It was reported that oxide 2DEG systems can change their properties under illumination.[2–4] To ensure the consistency and stability of the results, light exposure was kept to a minimum by keeping the samples in opaque boxes. Nonetheless, the strongest exposure to light was done under the wire bonding microscope. The samples used in Figure 2 underwent two sessions of bonding and measurement, to cover the necessary configurations (Hall measurements in two configurations and 4-point resistivity in two configurations). We used this process to estimate the stability of the samples under illumination, by keeping one of the wire configurations (resistivity along one direction) unchanged between the two bonding sessions. This configuration was measured after each bonding, and the maximum variation was determined to be below 30%, ensuring reasonable stability of the samples under light and ambient exposure.

Mobility

The mobility of most samples exhibits the classical temperature dependence of STO and STO-based 2DEGs[5,6]. The 40 and 50 sec samples show a slight deviation from this trend, with a possible source being a somewhat high contact resistance.

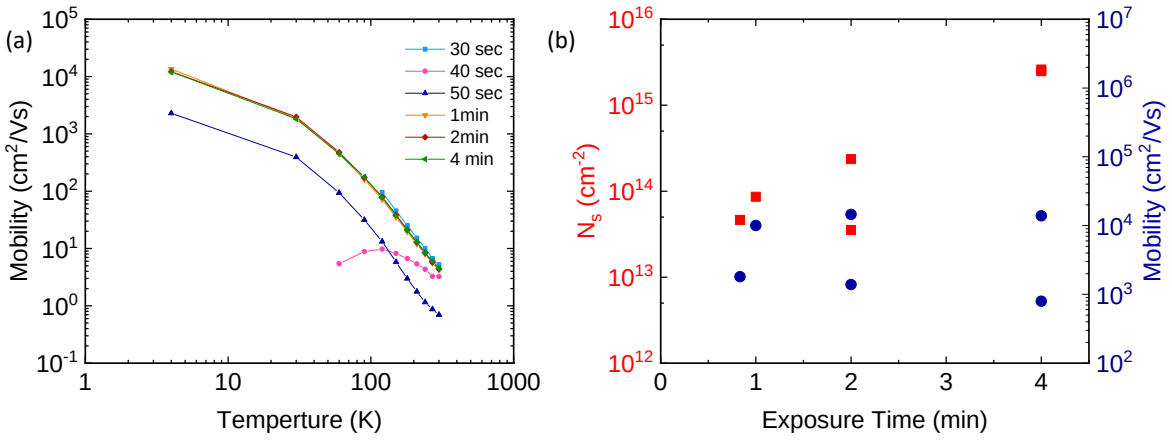

Figure S3. (a) The Hall mobility as a function of temperature for different NH_3 plasma duration. For 4 min and 4 K μ was estimated assuming one channel conduction by the slope at low field (see text for details). (b) Charge carrier density and mobility at 4 K as a function of the exposure duration. The 2 and 4 min data features two values of Ns and mobility, originating from the two carrier types (to be discussed in the next section).

Two channel fitting of the Hall Data

We fitted Hall data of all the metallic samples (t ≥ 50 sec) with one- and two-channel models. Here we present the two-channel model[7,8] – data and fit for these metallic samples at 4K (Fig. S3). The asymmetric MR and Hall curves resulting from contact asymmetry were aligned by averaging the forward and backward sweeps. The MR values were multiplied by π/ln(2).

The two-band fit is carried out by simultaneous fitting MR(B=0T) and R_{xy}(B) to the general expressions for parallel conducting systems with two subband contributions: [9]

$$MR = \frac{D_1 + D_2}{(D_1 + D_2)^2 + (A_1 + A_2)^2}$$

and

$$R_{xy} = \frac{A_1 + A_2}{(D_1 + D_2)^2 + (A_1 + A_2)^2}$$

where $D_i = \frac{n_i e^2 \tau_{t,i}}{m_i^*} \frac{1}{1+\omega_{c,i}^2 \tau_{t,i}^2}$ and $A_i = \frac{n_i e^2 \tau_{t,i}}{m_i^*} \frac{\omega_{c,i} \tau_{t,i}}{1+\omega_{c,i}^2 \tau_{t,i}^2}$. Here n_i is the carrier density of band i, e is the electronic charge, m_i^* is the carrier effective mass, $\tau_{t,i} = \mu_i m_i^*/e$ is the transport lifetime with μ_i being the mobility. Lastly the cyclotron frequency is $\omega_{c,i} = eB/m_i^*$ at magnetic field B.

Since other sources than 2-band contributions to the MR curve can arise at finite B-fields, we only fitted the MR(B=0T). The fitting routine then employed a 100 times iterative error minimization search varying the four fitting parameters (n_1, n_2, μ_1, μ_2) in order to find the best fit to the MR(0T) and Rxy(B) data.

For the 2 min sample, since the Hall curve (Fig. S3e) is very close to linear, we consider the single channel picture to be more appropriate, and we consider “channel 1” to be negligible.

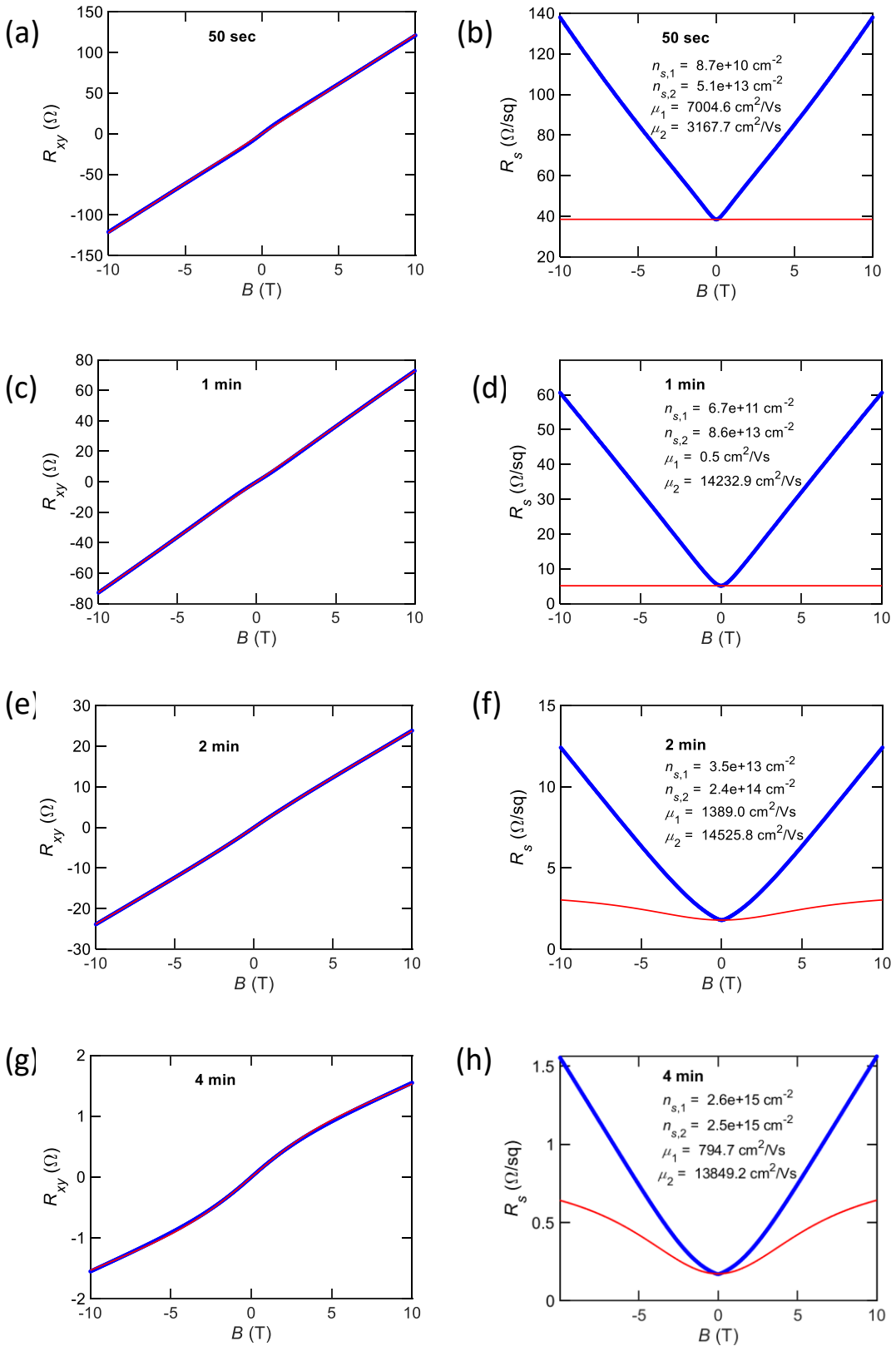

Figure S4. Hall and MR data (thick blue) and two-channel fits (thin red) for the metallic samples at 4K. (a) Hall and (b) MR for the 50 second sample. (c) Hall and (d) MR for the 1 minute sample. (e) Hall and (f) MR for the 2 minute sample. (g) Hall and (h) MR for the 4 minute sample.

Ti 2p XPS fitting parameters

Table S2. Fitting parameters for the Ti $2p_{3/2}$ peak for the various plasma durations, which were used for generating Figure 4b. The full raw dataset is enclosed as an xlsx file alongside the online Supporting Information.

	Ti2p 3/2 +4			Ti2p 3/2 +3				Ti2p 3/2 +2			
	pos	FWHM	%Area	pos	FWHM	offset	%Area	position	FWHM	offset	%Area
0 sec	471.20	0.92	100				0				0
30 sec	459.03	1.01	78.41	457.54	1.44	-1.49	16.03	456.16	1.49	-2.87	5.56
40 sec	459.38	1.08	75.37	457.91	1.50	-1.47	17.44	456.68	1.45	-2.70	7.19
50 sec	459.07	1.00	75.33	457.61	1.49	-1.46	18.82	456.13	1.30	-2.94	5.85
1 min	459.46	1.01	71.65	457.98	1.63	-1.48	22.54	456.62	1.49	-2.84	5.81
2 min	459.48	1.00	58.5	458.02	1.52	-1.46	34.1	456.44	1.41	-3.04	7.39
4 min	459.33	1.08	45.84	457.85	1.37	-1.49	46.2	456.37	1.52	-2.96	7.97

Ruling out nitrogen incorporation from NH_3

Since NH_3 plasma was used for the surface reduction process, we considered the possibility of Nitrogen incorporation at the Al_2O_3/STO interface during the pretreatment. No evidence of an N 1s peak was observed in any of the samples, within the sensitivity of XPS (~1% at.), Figure S4. We conclude that NH_3 contributes to the conductivity only by surface reduction.

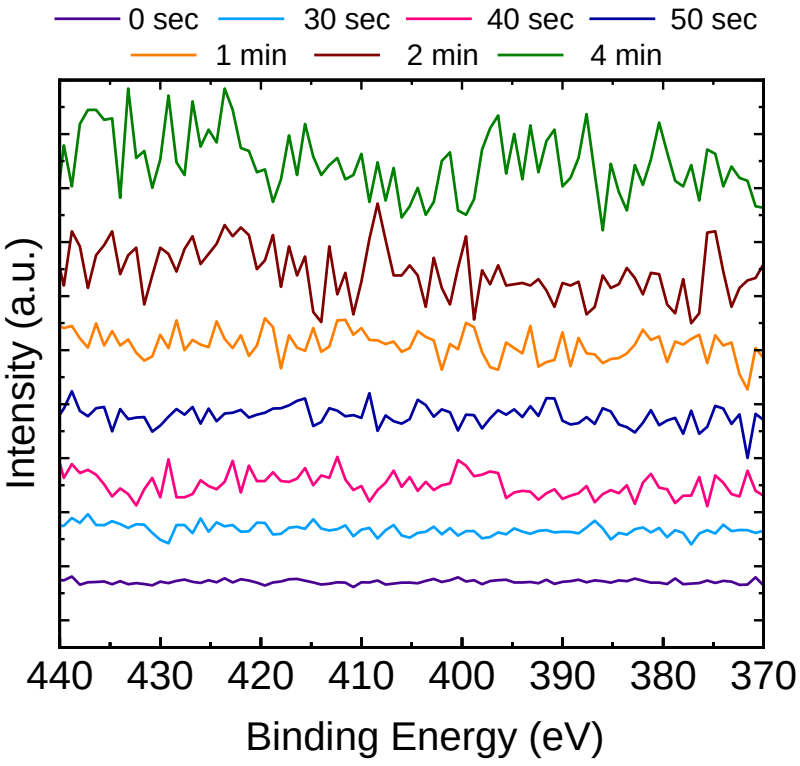

Figure S5. XPS spectrum of N 1s spectral region for different plasma exposure durations.

Bibliography

[1] K. Wolff, R. Schäfer, D. Arnold, R. Schneider, M. Le Tacon, and D. Fuchs, J. Appl. Phys. **128**, (2020).
[2] S. Su, H. Gao, Y. Shen, W. Peng, and X. Zhu, Appl. Phys. Lett. **115**, 151601 (2019).
[3] M.C. Tarun, F.A. Selim, and M.D. McCluskey, Phys. Rev. Lett. **111**, 187403 (2013).
[4] A. Tebano, E. Fabbri, D. Pergolesi, G. Balestrino, and E. Traversa, ACS Nano **6**, 1278 (2012).
[5] A. Verma, A.P. Kajdos, T.A. Cain, S. Stemmer, and D. Jena, Phys. Rev. Lett. **112**, 216601 (2014).
[6] F. Trier, D. V Christensen, and N. Pryds, J. Phys. D. Appl. Phys. **51**, 293002 (2018).
[7] E.N. Jin, A. Kakekhani, S. Ismail-Beigi, C.H. Ahn, and F.J. Walker, Phys. Rev. Mater. **2**, 115001 (2018).
[8] B. Leikert, J. Gabel, M. Schmitt, M. Stübinger, P. Scheiderer, L. Veyrat, T.L. Lee, M. Sing, and R. Claessen, Phys. Rev. Mater. **5**, 1 (2021).
[9] M. van der Burgt, V.C. Karavolas, F.M. Peeters, J. Singleton, R.J. Nicholas, F. Herlach, J.J. Harris, M. Van Hove, and G. Borghs, Phys. Rev. B **52**, 12218 (1995).